Bifurcation analysis of parametrically excited inclined cable close to two-to-one internal resonance.

M.R. Marsico[1,a], V. Tzanov[a], D.J. Wagg[a], S.A. Neild[a], B. Krauskopf[a]

[a] *Faculty of Engineering, University of Bristol, Queens Building, University Walk, Bristol BS8 1TR, U.K.*

Citation: *Journal of Sound and Vibration* **330**:*6023–6035, 2011.*
http://dx.doi.org/10.1016/j.jsv.2011.07.027

Abstract

This paper presents a study of how different vibration modes contribute to the dynamics of an inclined cable that is parametrically excited close to a 2 : 1 internal resonance. The behaviour of inclined cables is important for the design and analysis of cable-stay bridges. In this work the cable vibrations are modelled by a four-mode model. This type of model has been used previously to study the onset of cable sway motion caused by internal resonances which occur due to the nonlinear modal coupling terms. A bifurcation study is carried out with numerical continuation techniques applied to the scaled and averaged modal equations. As part of this analysis, the amplitudes of the cable vibration response to support inputs is computed. These theoretical results are compared with experimental measurements taken from a 5.4 m long inclined cable with a vertical support input at the lower end. In general this comparison shows a very high level of agreement.

Key words: Cable vibration, internal resonance, sway motion, modal interaction, bifurcation analysis.

1. Introduction

Inclined cables are used to support the bridge deck in cable-stay bridges. The cables are typically lightly damped, and when the bridge deck oscillates it

Email address: m.r.marsico@bristol.ac.uk (M.R. Marsico)

provides a support motion input to the cable. This type of excitation can lead to large amplitude vibrations of the cable [1]. A case of particular interest is when an internal resonance occurs between the in-plane and out-of-plane modes of vibration of the cable. This phenomenon was studied in [2] by using nonlinear Mathieu-type equations to model parametric resonance between the in-plane and out-of-plane modes of vibration of the cable [3, 4, 5, 6]. The most significant resonance occurs when the associated modal frequencies of the second in-plane and first out-of-plane mode are at a ratio of $2:1$. Close to resonance, relatively small deck inputs are sufficient to trigger the out-of-plane sway motion of the cable. This onset of sway motion can be formulated as a stability problem. In this case, zero sway motion is considered a stable situation, and the onset of sway motion can be interpreted as the loss of stability of the zero solution. This approach has been considered by many authors; see for example [7, 8, 9, 10, 11, 12, 13, 14, 15] and references therein. The general formulations for cable dynamics are discussed in [16, 17].

In this paper the Warnitchai equations [18] (see also [19] for a detailed derivation) are used to model the vibration of the cable. It is assumed that the longitudinal vibrations of the cable can be neglected, so that the planes of interest are vertical (in-plane) and sway (out-of-plane). Four modes are included in the model, two in-plane and two out-of-plane, which enables the important low frequency dynamic behaviour to be modelled [11, 12]. The Warnitchai equations are scaled and averaged using the same procedure as previously presented in [13, 14, 22]. Then a bifurcation study is carried by means of numerical continuation [20] with the software package AUTO [21]. In this way, the stability boundaries for the zero-sway solution can be computed in the form of a series of resonance (or Arnold) tongues. The discussion concentrates on the $2:1$ resonance tongue; additional resonances are discussed in [14]. Furthermore, by using AUTO, coupled solution branches that involve non-zero out-of-plane solutions are detected and their stability properties identified.

In addition to computing the resonance tongues [23, 24, 25], here, amplitude information within the tongue is also computed and compared to experimental results. These experimental test were carried out on an inclined 5.4 m long cable [26]. The modal data from the model was transformed into displacement values for the mid and quarter points of the experimental cable. When compared, the simulation and experimental results show a high level of agreement for most parts of the curves [27]. A discrepancy between simulated and experimental results occurs close to tip of the resonance tongue

where more complex dynamic effects are expected to occur. Such effects are not fully captured by the four mode model, but can be explained using the results of the bifurcation study.

The remainder of this paper is structured as follows. In Section 2 the equations of motion for the inclined cable model are presented as derived via scaling and first-order averaging. Section 3 describes the experimental set-up and tests conducted in the laboratory. Section 4 describes the bifurcation study and numerical continuation analysis, as well as a comparison with experimental measurements. Conclusions are drawn in Section 5.

2. The theoretical model

The modal equations of motion for an inclined taut cable derived by Warnitchai *et al.* [18] are used here as the basis for the theoretical investigation. These modal equations are then scaled and averaged as described in [13, 14] (see also [19] for a description of the averaging technique) to give equations relating to the amplitude of response of each mode. The averaged equations are the basis for the bifurcation study described in Section 4. For completeness, we set out the main steps of this derivation.

A schematic of the cable is shown in Fig. 1, where v and w are out-of-plane (sway) and in-plane (transverse) displacements of the cable, respectively, and θ is the angle of inclination measured from the horizontal line in the gravity plane. Axial vibrations of the cable are neglected in this model since they occur at much higher frequencies. The cable is rigidly supported at the upper end and a vertical support input is included at the lower end.

2.1. Modal equations

In the Warnitchai *et al* [18] derivation, the dynamic response of the cable is split into a quasi-static motion (which ensures that the moving boundary condition at the lower support is met by considering the movement of a mass-less tendon between the supports) and a modal response

$$\begin{aligned} v_d(x,t) &= v_m(x,t) = \sum_{n=1}^{\infty} \phi_n(x) y_n(t), \\ w_d(x,t) &= w_q(x,t) + w_m(x,t) = w_q(x,t) + \sum_{n=1}^{\infty} \psi_n(x) z_n(t), \end{aligned} \tag{1}$$

where the subscripts d, q and m relate to dynamic, quasi-static and modal displacements, respectively, the spatial functions $\phi(x)$ and $\psi(x)$ are the in-plane and out-of-plane linear modeshapes of a cable with fixed ends, and $y_n(t)$ and $z_n(t)$ their corresponding time-dependent generalised coordinates. The in-plane quasi-static motion is given by

$$w_q = \delta\cos(\theta)\left(\frac{x}{\ell}\right) - \frac{\gamma E_q \ell\delta\sin(\theta)}{2\sigma_s^2}\left[\left(\frac{x}{\ell}\right) - \left(\frac{x}{\ell}\right)^2\right], \tag{2}$$

where the second term on the right-hand side is due to the change in the tension in the cable affecting the static sag of the cable [18, 19]. Furthermore, σ_s is the static stress acting along the x-axis and

$$E_q = \frac{1}{1+\lambda^2/12}E, \quad \text{with} \quad \lambda^2 = \frac{E}{\sigma_s}\left(\frac{\gamma\ell}{\sigma_s}\right)^2, \quad \gamma = \rho g\cos\theta, \tag{3}$$

where λ^2 is Irvine's parameter [16]. The system may be linearized assuming that the sag is small compared to the length of the cable, the dynamics along the cable are insignificant and the amplitude of vibration is small compared with the sag [28]. By using the modal decomposition as the mode shapes of this linearized system, the Galerkin technique can be used to derive the modal equations of motion for the nonlinear cable dynamics [29]; here the assumption that the amplitude of vibration is small compared to the sag is relaxed by using a nonlinear compatibility expression. The resulting modal representation of the out-of-plane cable motion for the n^{th} mode may be expressed as

$$\begin{gathered} m_{yn}\left(\ddot{y}_n + 2\xi_{yn}\omega_{yn}\dot{y}_n + \omega_{yn}^2 y_n\right) + \sum_k \nu_{nk} y_n\left(y_k^2 + z_k^2\right) + \\ \sum_k 2\beta_{nk} y_n z_k + 2\eta_n\sin(\theta)\delta y_n = 0, \end{gathered} \tag{4}$$

and the in-plane cable motion as

$$\begin{gathered} m_{zn}\left(\ddot{z}_n + 2\xi_{zn}\omega_{zn}\dot{z}_n + \omega_{zn}^2 z_n\right) + \sum_k \nu_{nk} z_n\left(y_k^2 + z_k^2\right) + \\ \sum_k 2\beta_{nk} z_n z_k + \sum_k \beta_{kn}\left(y_k^2 + z_k^2\right) + 2\eta_n\sin(\theta)\delta z_n + \\ \zeta_n(-1)^{n+1}\cos(\theta)\ddot{\delta} - \alpha_n\sin(\theta)\ddot{\delta} = 0. \end{gathered} \tag{5}$$

In these equations $m_{yn} = m_{zn} = m = \rho A\ell/2$ is the effective mass and the parameters ν_{nk}, β_{nk}, η_n, ζ_n and α_n are given by

$$\nu_{nk} = \frac{EA\pi^4 n^2 k^2}{8\ell^3}, \quad \beta_{nk} = \frac{EA\pi\gamma n^2}{4\ell\sigma_s}\left(\frac{1+(-1)^{k+1}}{k}\right), \quad \eta_n = \frac{E_q A\pi^2 n^2}{4\ell^2},$$
$$\zeta_n = \frac{2m}{n\pi}, \quad \alpha_n = \frac{2m\gamma\ell E_q}{n^3\pi^3\sigma_s^2}\left(1+(-1)^{n+1}\right). \tag{6}$$

Where A is the cross section area of the cable. The mode shapes for the out-of-plane and even in-plane modes of the linearized system are given by

$$\phi_n = \sin\left(n\pi\frac{x}{\ell}\right) \qquad \text{for} \quad n = 1, 2, 3, \ldots, \tag{7}$$
$$\psi_n = \sin\left(n\pi\frac{x}{\ell}\right) \qquad \text{for} \quad n = 2, 4, 6, \ldots. \tag{8}$$

For the odd in-plane modes the mode shapes are more complex; however, as is discussed in [19], for taut cables they may be approximated to sine functions of the same form as the out-of-plane modes. Finally, the out-of-plane and in-plane natural frequencies, ω_{yn} and ω_{zn}, respectively, are given by

$$\omega_{yn} = \frac{n\pi}{\ell}\sqrt{\frac{\sigma_s}{\rho}}, \quad \omega_{zn} = \frac{n\pi}{\ell}\sqrt{\frac{\sigma_s}{\rho}(1+k_n)}. \tag{9}$$

Here k_n is due to the effect of sag and given by

$$k_n = \left(\frac{2\lambda^2}{\pi^4 n^4}\right)\left(1+(-1)^{n+1}\right)^2, \tag{10}$$

assuming a sinusoidal mode shape.

The study presented here concentrates on forcing frequencies close to the second natural frequency $\Omega \approx \omega_{z2} = \omega_{y2}$. This can trigger the $2:1$ resonance case in the first in- and out-of-plane modes due to the nonlinear nature of the system. Therefore, these four modes will be considered. Note that $\omega_{y1} = \omega_{z2}/2$ and ω_{z1} are slightly larger than half the second natural frequency.

2.2. Scaling and averaging

The technique of scaling and averaging (see for example [19, 30]) is now applied to the four modal equations of motion in- and out-of-plane for $n =$

1, 2. We review here the three steps in this procedure; details can be found in [13, 14].

Step 1 Each modal equation is written in the standard Lagrange form [30]

$$\ddot{v}_i + \omega_{vi}^2 v_i = \epsilon f_i(v_1, v_2, v_3, v_4, \dot{v}_1, \dot{v}_2, \dot{v}_3, \dot{v}_4, \delta, \ddot{\delta}), \tag{11}$$

where $\{v_1, v_2, v_3, v_4\} = \{y_1, z_1, y_2, z_2\}$ and $\{\omega_{v1}, \omega_{v2}, \omega_{v3}, \omega_{v4}\} = \{\omega_1, \omega_1, 2\omega_1, 2\omega_1\}$ with $\omega_1 = \omega_{y1}$. In this formulation the small parameter ϵ has been introduced, indicating that the damping and nonlinear terms are assumed to be small. Equations for the functions f_i can be derived by comparing Eqs. 4 and 5 with Eq. 11. Note for the case of $i = 2$, f_2 contains the frequency detuning term $-\hat{k}_1\omega_1^2 z_1$ where, since k_1 is small, k_1 has been expressed as $k_1 = \epsilon\hat{k}_1$ (recalling that $\omega_{z1} = \omega_1\sqrt{1+k_1}$).

Step 2 Because the forcing is close to the second natural frequency of the cable, the forcing frequency Ω is written as $\Omega = 2\omega_1(1+\mu)$ where μ is the frequency detuning parameter, which may be expressed as $\mu = \epsilon\hat{\mu}$ since it is small. Applying the time transform $\tau = t(1+\mu)$ allows Eq. 11 to be rewritten as

$$v_i'' + \omega_{vi}^2 v_i = \epsilon[f_i(v_1, v_2, v_3, v_4, v_1', v_2', v_3', v_4', \delta, \delta'') + 2\hat{\mu}\omega_{vi}^2 v_i] = \epsilon g_i, \tag{12}$$

where $\{\}'$ is the derivative with respect to τ and the terms of order ϵ^2 have been ignored.

Step 3 Making substitutions of the form

$$v_i = v_{ic}\cos(\omega_{vi}\tau) + v_{is}\sin(\omega_{vi}\tau), \quad v_i' = \omega_{vi}[-v_{ic}\sin(\omega_{vi}\tau) + v_{is}\cos(\omega_{vi}\tau)] \tag{13}$$

into Eq. 12 results in equations for the dynamics of the amplitude content of the modes

$$v_{ic}' = -\frac{\epsilon}{\omega_{vi}}\sin(\omega_{vi}\tau)g_i, \quad v_{is}' = \frac{\epsilon}{\omega_{vi}}\cos(\omega_{vi}\tau)g_i \tag{14}$$

(see [19, 30]). Since Eq. 14 indicates that the derivatives of v_{ic} and v_{is} are small (of order ϵ^1) the equations can be averaged. Specifically, this means that the equations are averaged over a period of oscillation at frequency ω_1 while treating the v_{ic} and v_{is} terms within g_i as constant over the oscillation. This averaging over a period of oscillation at frequency ω_1 in the transformed

τ-time domain is equivalent to averaging over two periods of oscillation at frequency Ω in the t-time domain.

The resulting averaged equations are:

$$
\begin{aligned}
y'_{1c} &= \left(\frac{W_{12}z_{1c}z_{1s}}{16\omega_1} - \xi\omega_1\right)y_{1c} - \left(\mu\omega_1 + \frac{N_1\Delta}{4\omega_1} - \frac{W_{12}}{32\omega_1}\left(C_1 - 2z_{1c}^2\right)\right)y_{1s},\\
y'_{1s} &= \left(\mu\omega_1 - \frac{N_1\Delta}{4\omega_1} - \frac{W_{12}}{32\omega_1}\left(C_1 - 2z_{1s}^2\right)\right)y_{1c} - \left(\xi\omega_1 + \frac{W_{12}z_{1c}z_{1s}}{16\omega_1}\right)y_{1s},\\
y'_{2c} &= \left(\frac{W_{12}z_{2c}z_{2s}}{2\omega_1} - 2\xi\omega_1\right)y_{2c} - \left(2\mu\omega_1 - \frac{W_{12}}{8\omega_1}\left(C_2 - 4z_{2c}^2\right)\right)y_{2s},\\
y'_{2s} &= \left(2\mu\omega_1 - \frac{W_{12}}{8\omega_1}\left(C_2 - 4z_{2s}^2\right)\right)y_{2c} - \left(2\xi\omega_1 + \frac{W_{12}z_{2c}z_{2s}}{2\omega_1}\right)y_{2s},\\
z'_{1c} &= \left(\frac{W_{12}y_{1c}y_{1s}}{16\omega_1} - \xi\omega_1\right)z_{1c} - \left((\mu-\kappa)\omega_1 + \frac{N_1\Delta}{4\omega_1} - \frac{W_{12}}{32\omega_1}\left(C_1 - 2y_{1c}^2\right)\right)z_{1s},\\
z'_{1s} &= \left((\mu-\kappa)\omega_1 - \frac{N_1\Delta}{4\omega_1} - \frac{W_{12}}{32\omega_1}\left(C_1 - 2y_{1s}^2\right)\right)z_{1c} - \left(\xi\omega_1 + \frac{W_{12}y_{1c}y_{1s}}{16\omega_1}\right)z_{1s},\\
z'_{2c} &= \left(\frac{W_{12}y_{2c}y_{2s}}{2\omega_1} - 2\xi\omega_1\right)z_{2c} - \left(2\mu\omega_1 - \frac{W_{12}}{8\omega_1}\left(C_2 - 4y_{2c}^2\right)\right)z_{2s},\\
z'_{2s} &= \left(2\mu\omega_1 - \frac{W_{12}}{8\omega_1}\left(C_2 - 4y_{2s}^2\right)\right)z_{2c} - \left(2\xi\omega_1 + \frac{W_{12}y_{2c}y_{2s}}{2\omega_1}\right)z_{2s} - B\Delta\omega_1,
\end{aligned}
\tag{15}
$$

where $M_1 = y_{1c}^2+y_{1s}^2+z_{1c}^2+z_{1s}^2$, $M_2 = y_{2c}^2+y_{2s}^2+z_{2c}^2+z_{2s}^2$, $C_1 = 3M_1+8M_2$ and $C_2 = M_1 + 6M_2$. Furthermore, $\kappa = k_1/2$, $W_{nk} = \nu_{nk}/m$, $N_n = 2\eta_n \sin\theta/m$, $B = \zeta_2 \cos\theta/m$ and $\delta = \Delta\cos(\Omega t)$; see Table 1.

3. Experimental cable set-up

Having defined the analytical model, we now introduce the physical cable experiment that was used for this study [31, 32]. The inclined cable used in the experimental tests for this study is shown in Fig. 2. It is 5.4 m long, has diameter 0.78 mm and is inclined at 22.6°. To improve the scaling characteristics of the cable, 21 lead masses have been added to increase its

mass. The masses are spaced every 250 mm, except the first and the last ones which have distance 200 mm from each end; Fig. 2b. As the analysis is restricted to only the first and second modes, the added masses do not play a significant role in modifying the mode shapes and can be considered as equivalent to a distributed weight along the cable.

The masses are also used in the acquisition of data during the experimental tests, namely as targets that the high-speed camera system follows. Specifically, two masses — one in the middle and the other a quarter distance along the cable — are used to measure the vibration of the cable. This data is acquired using an Imetrum Video Gauge System (VGS) consisting of two cameras, one to record in-plane motion and the second to capture the out-of-plane motion.

The cable is fixed at the top where it is possible to adjust the static tension prior to each test, and all results shown here are for a value of T_s=286 N. At the lower end the cable is connected to a short steel beam via a multiaxial (six DoF) load cell and a vertical LVDT (linear variable differential transformer) with limit displacement of $\pm 10mm$. The actuator, shown in Fig. 2c, has 10 kN maximum force and $\pm 150mm$ displacement. The hydraulic system uses an oil pump with 100 l/min capacity and pressure of 23 MPa.

The system used for the input and output data involves three computers. Computer 1 is used to control the hydraulic actuator, and this is where the required forcing amplitude and frequency for different kinds of tests can be specified. Computer 2 is used for data acquisition of all instruments except the VGS. The third computer is used to record the motion of the cable from the VGS.

During a test, the actuator imitates the deck motion and excites the cable with a sine wave input. Data is recorded using the VGS, load cell and LVDT. The data is post-processed to compute the steady-state amplitudes for the mid- and quarter-point cable displacements in both the in- and out-of-plane directions. Two important quantities are measured in the experiment: (i) the forcing amplitude value at which any out-of-plane motion begins, and (ii) the steady state maximum amplitude per forcing period. A discussion of how this experimental data compares with a bifurcation analysis of the scaled, averaged model is given in the next section.

4. Bifurcation study

The connection between the solutions of system of Eqs. (15) and the vibration response of the cable is given by the amplitude contributions of the four different modal amplitudes, which are defined as:

- $Z_2 = \sqrt{z_{2c}^2 + z_{2s}^2}$ for the second in-plane modal amplitude;
- $Z_1 = \sqrt{z_{1c}^2 + z_{1s}^2}$ for the first in-plane modal amplitude;
- $Y_2 = \sqrt{y_{2c}^2 + y_{2s}^2}$ for the second out-of-plane modal amplitude;
- $Y_1 = \sqrt{y_{1c}^2 + y_{1s}^2}$ for the first out-of-plane modal amplitude.

The main parameters of interest of the system of Eqs.(15) are the amplitude of excitation Δ (measured in metres) and the detuning μ between the frequency of the actuator and the second natural frequency of the cable. In order to work with non-dimensional values for the actuator amplitude, we consider throughout the normalized quantity Δ/L, where L is the untensioned length of the cable which was $L = 5.4$ m in the experiment, here $L = \ell$ the support separation distance.

Our goal now is to investigate how the contributions of the different modal amplitudes Z_2, Z_1, Y_2 and Y_1 of Eqs. (15) change as a function of Δ and μ. To this end, we present in Figs. 3 and 4 stability diagrams in the $(\mu, \Delta/L)$-plane that explain how the different modal amplitudes contribute to the overall behavior. The curves in Figs. 3 and 4 represent transitions that are due to changes of stability of individual modal amplitudes; they have been computed with the numerical continuation package AUTO [21]. These transitions are known bifurcations [33, 34], and we find two types of bifurcations in the region of interest $(\mu, \Delta/L) \in [0, 0.0015] \times [-0.03, 0.07]$. The first is the saddle-node (or fold) bifurcation, where a stable and an unstable branch of solutions meet; secondly, we find branch point bifurcations that correspond to the onset of a further modal amplitude which then contributes to the solution.

Figure 3 shows loci of fold bifurcation points of the Z_2-amplitude as the grey curve labelled F_{Z_2}, as well as black curves B_{Y_1} and B_{Z_1} of branch point bifurcations of the Y_1-amplitude and of the Z_1-amplitude, respectively. These bifurcations are observable because they correspond to stable solutions. In the lower region (below these curves) the stable solution of Eqs. (15) has only a contribution of the Z_2-amplitude (that is, $Z_1 = Y_2 = Y_1 = 0$), meaning that the response of the cable consists of purely the second in-plane mode. When

the curve F_{Z_2} (between the points C and K) is crossed as Δ/L is increased, we encounter the fold bifurcation and this stable solution disappears. As a consequence, there is a sudden transition to an entirely different stable solution that has contributions of the Z_2-amplitude and both the Y_2-amplitude and the Y_1-amplitude, meaning that the cable now features out-of-plane motion. How this new solution arises is discussed in Section 4.1 below. Crossing a branch point bifurcation curve in Fig. 3 has less dramatic consequences. When the curve B_{Z_1} is crossed for increasing Δ/L one finds an onset of the contribution of the Z_1-amplitude, while still $Y_2 = Y_1 = 0$; hence, the cable dynamics is still in-plane. Similarly, when the curve B_{Y_1} is crossed for increasing Δ/L the Y_1-amplitude starts to contribute, while still $Z_1 = Y_2 = 0$; in other words, one observes the onset of the first out-of-plane modal amplitude. Time series plots either side of the B_{Y_1} curve are shown in [13] for a three-mode model.

The bifurcation curves shown in Fig. 3 are the transition curves that one encounters first in the experiment when Δ/L is increased for fixed detuning μ. Indeed, these curves agree well with the experimental measurements. The squares are the last measured points where $Z_1 = Y_2 = Y_1 = 0$, and the triangle where a contribution $Y_1 \neq 0$ of the first out-of-plane Y_1-amplitude was identified for the first time (when increasing Δ/L). Similarly, the diamonds indicate that a non-zero contribution of the first in-plane Z_1-amplitude was first observed. Given the gradual onset of the corresponding modal amplitudes, these measurements points agree well with the curves B_{Z_1} and B_{Y_1}, respectively.

How the curves shown in Fig. 3 arise can only be understood when they are considered as part of a stability diagram that also shows bifurcation curves that correspond to unstable solutions which arise from pure Z_2-solutions. This is shown in Fig. 4, where the curves F_{Z_2}, B_{Z_1}, B_{Y_2} and B_{Y_1} are seen to form a complicated structure. Throughout, parts of curves that correspond to bifurcation of stable solutions are drawn as solid curves, while parts of curves that correspond to bifurcations of unstable solutions are dashed. Notice the solid curves from Fig. 3 are parts of the corresponding bifurcation curves. More specifically, the fold curve F_{Z_2} has a cusp point C and extends past the point K, where it meets the curve B_{Z_1}; apart from the part of F_{Z_2} between C and K that was shown in Fig. 3. Note also the part of curve F_{Z_2} between C and the point P corresponds to the bifurcation of a stable solution. However, this fold bifurcation is almost immediately followed by the curve B_{Y_2} of branch point bifurcations of the second out-of-plane

Y_2-amplitude.

Notice that the curve B_{Y_2} is solid and corresponds to bifurcations of an attracting solution; see the enlargement in Fig. 4b showing $(\mu, \Delta/L) \in [0, 0.00011] \times [-0.03, 0.07]$. Hence, the region of stability of the stable solution in between F_{Z_2} from C to P and the solid part of B_{Y_2} is extremely narrow, and as a result it is very difficult to observe a stable solution with a contribution of only the Y_2-amplitude; this is why these solid parts of F_{Z_2} and B_{Y_2} are not shown in Fig. 3. Nevertheless, we detected the onset of the Y_2-amplitude in an experiment for $\mu = 0.02$; it is represented by the upside-down triangle. Notice further that the curves B_{Y_1} and B_{Z_1} extend past the points N and K, respectively, where they indicate that the corresponding modal amplitude starts to contribute to an unstable solution.

As the excitation is close to the cable's second natural frequency, Z_2-amplitudes persist in all the coupled responses that were observed. The bifurcation analysis shows three types of coupled responses, namely (Z_2, Z_1), (Z_2, Y_1), and (Z_2, Y_1, Y_2). For each value of μ, there is a value of Δ/L above which, only Y_1-amplitudes will be present in addition to the Z_2-amplitudes. In Fig. 3 these values are represented by the B_{Y_1}-branch point bifurcation curve where the stable Z_2-solutions meet (Z_2, Y_1)-solutions. For μ larger than 0.0036 on the right from the point N in Figs. 3 and 4, this transition is not direct and there are other coupled amplitudes that could be excited. Between N and K, the transition is to (Z_2, Y_1, Y_2)-amplitudes, while to the right of point K, first it will be (Z_2, Z_1) and then again (Z_2, Y_1, Y_2)-amplitudes. To clarify these transitions in Fig. 5, the stability diagram of (Z_2, Y_1, Y_2)-stable solutions in $(\mu, \Delta/L)$-plane is shown. It shows the borders of stable (Z_2, Y_1, Y_2)-solutions in the same way as Fig. 3 shows the borders of stable Z_2-solutions. The transition from (Z_2, Y_1, Y_2)-amplitudes to (Z_2, Y_1)-amplitudes occur at the branch point curve B^1. The latter arises from the same point N shown in Fig. 3. Also, in Fig. 5 the following bifurcation curves can be seen:

- F^1 and F^2 fold bifurcation curves and H^1 Hopf bifurcation curve, at which unstable (Z_2, Y_1, Y_2)-solutions meet stable (Z_2, Y_1, Y_2)-solutions;
- B^2 branch point bifurcation curve, at which stable (Z_2, Y_2)-solutions meet stable (Z_2, Y_1, Y_2)-solutions, where the first ones of these arises from B_{Y_2}-branch point curve, see Fig. 4.

In Fig. 5 the points N, M and Q represent the borders between the different bifurcation curves. Point R is cusp bifurcation point but because it is so close

to H^1, it looks like H^1 meets F^2 at R (which in the sense of this stability diagram could be assumed). Note the response amplitudes in (Z_2, Y_1, Y_2)-mode is not a pure 2:1 internal resonance. However, this type of internal resonance is a transition between the response in pure Z_2 modal amplitudes and 2:1 internal resonance between Z_2 and (Z_2, Y_1)-amplitudes, that occur for Δ/L large enough.

At the points N, K, P, M, Q different bifurcation curves cross each other, which indicates a bifurcation of codimension two [34]. As a result the nature of at least one of the bifurcation curves switches from involving a stable an unstable solution.

Overall, the bifurcation curves F_{Z_2}, B_{Z_1}, B_{Y_2} and B_{Y_1} from Fig. 3 and Fig. 4 also, B^1, B^2, F^1, F^2 and H^1 from Fig. 5 form a consistent stability perspective in the $(\mu, \Delta/L)$-plane that explains the nature of the transition from pure Z_2-response to coupled (Z_2, Y_1)-response. Finally, the overall solution structure can be represented by surfaces of solutions over the $(\mu, \Delta/L)$-plane, when an appropriate norm is used to represent the respective solutions; however this is beyond the scope of this paper.

4.1. Amplitudes of vibration

The stability diagrams in the $(\mu, \Delta/L)$-plane shown in Figs. 4 and 5 feature quite a number of bifurcation curves in the region of positive μ. Some of these bifurcations give rise to additional branches of stable solutions, which are connected to the known stable solutions discussed above by branches of unstable solutions.

In Figs. 3 and 4 all the bifurcation loci that could be detected when the pure Z_2-solutions are continued are shown. In [13, 14] the Z_2-bifurcation curves were obtained by using properties of the Jacobian matrix of the vector field, defined by the cable differential equations. Later the curves were examined experimentally and in simulations. In the present paper the coupled solutions that arise from the branch points of the non-coupled Z_2-solutions are followed by AUTO, as was done in [22]. In the present work, different types of solution branches were detected, the amplitudes that different modes add to the response were defined and then, the displacements of the cable were predicted.

These solution branches that involve non-zero out-of-plane solutions, can be seen in Fig. 6 which shows the one-parameter bifurcation diagram of Eqs. (15) for fixed $\mu = 0.02$; here solution branches, computed by numerical continuation in Δ/L, are represented by the norm $||N|| = \sqrt{Z_1^2 + Z_2^2 + Y_1^2 + Y_2^2}/L$

(which measures contributions from all four modal amplitudes of the cable). Stable parts of solution branches are shown as black curves, and unstable parts as grey curves. The continuation started for Δ/L by following the solution curve l_1, where only the second in-plane amplitude Z_2 has a contribution to the vibration response of the cable. At Δ/L approximately 1.56×10^{-4} a branch point B_1 to another solution branch l_2 is detected; beyond this point the solution curve l_1 becomes unstable, while the branch l_2 is stable, where the first in-plane amplitude Z_1 has a contribution as well as Z_2. At Δ/L approximately 1.8781×10^{-4} there is branch point B_2 where l_2 and l_1 meet and branch l_1 regains stability until the fold point F_1 is reached.

In terms of the dynamics of the cable, moving Δ/L beyond 2.0372×10^{-4} there is a jump to another stable solution branch, namely the branch l_3 where we find responses from all the modal amplitudes considered except Z_1. The shaded area in Fig. 5 is made by branches, like l_3, that involve stable (Z_2, Y_1, Y_2)-solutions. At Δ/L approximately 3.9989×10^{-4} a branch point B_3 is detected where l_3 meets the solution branch l_4, along which the first out-of-plane modal amplitude Y_1 is coupled with Z_2. This branch is stable until the branch leaves the Δ/L range of interest in Fig. 6. Note that the stable branches l_3 and l_4 are connected to the stable branches l_1 and l_2 via branches of unstable solutions. More specifically, there is an unstable part of l_1 that extends beyond the fold point F_1 and past a second fold point F_2. Near F_2 one finds a branch point bifurcation to an unstable branch where the modal amplitudes Y_2 and Z_2 contribute. This unstable branch is connected to the stable l_3 by the Hopf bifurcation point $H \in H^1$ (see Fig. 5). Finally, the unstable part of l_4, to the left of the branch point $B_3 \in B^1$ extends past a fold bifurcation and connects to the former branch. The fact that all of these branches are connected allowed us to continue them (irrespective of their stability), yielding an consistent one-parameter bifurcation diagram. It is a particular strength of the continuation approach that new branches of (stable) solutions can be found in a systematic fashion. It should be noted that Fig. 6 shows the solution branches that are connected to the zero excitation amplitude solution of Eqs. (15) for fixed μ. In the region of interest, other solutions may be found that do not intersect with the ones shown in Fig. 6.

In order to facilitate the physical interpretation of the stable branches, Fig. 7 shows the contributions of Z_2, Z_1, Y_2, and Y_1 modal amplitudes to the stable branches l_1–l_4 in separate panels. This allows us to see clearly how much a particular modal amplitude contributes to the cable steady-state

vibration response. As Fig. 7a shows, the modal amplitude Z_2 contributes to all stable branches; as Δ/L grows, the response of the cable in Z_2 grows until the fold point F_1 is reached. The contributions of all other modal amplitudes are zero, except for a small contribution of Z_1 along the branch l_2; see Fig. 7b. As was mentioned before, when Δ/L is increased beyond F_1, the only available stable solutions is that on branch l_3, which features strong contributions from Y_2 and Y_1; see Figs. 7c and d. The contribution of Y_2 then vanishes when the branch point B_3 is reached, and along the branch l_4 only the modal amplitudes Z_2 and Y_1 are active. Notice that at the frequency considered $\mu = 0.02$, except along the small branch l_2, the modal amplitude Z_1 does not contribute to the stable dynamics of the cable.

4.2. Comparison between analysis and experiment

The experimental parameters are given in [14]. The Young's modulus of the steel cable was very slightly modified from the standard assumued value of 210GPa to best fit the first in-plane natural frequency resulting in a modified value of214GPa being used. This resulted in excellent agreement of the first four natural frequencies in both planes, the first two of which in each plane are shown in Table 2.

In the experiments we measure the amplitudes of the in-plane displacement w and the out-of-plane displacement v at the mid-point and the quarter point of the cable, we define their maximums with W and V respectively. Each test has been repeated five times to ensure accurate measurement. The measurement variation is in the order of 1-2%.

To allow for a comparison between our bifurcation analysis and experimental data we show in Fig. 8 the stable branches in terms of the maximal

displacements as given by

$$\begin{aligned}
\frac{W}{L}\left(\frac{L}{4},\Delta\right) &= \frac{Z_1}{\sqrt{2}L}(\Delta)+\frac{Z_2}{L}(\Delta)+\frac{w_q}{L}\left(\frac{L}{4},\Delta\right), \qquad (16)\\
\frac{W}{L}\left(\frac{L}{2},\Delta\right) &= \frac{Z_1}{L}(\Delta)+\frac{w_q}{L}\left(\frac{L}{2},\Delta\right),\\
\frac{V}{L}\left(\frac{L}{4},\Delta\right) &= \frac{Y_1}{\sqrt{2}L}(\Delta)+\frac{Y_2}{L}(\Delta),\\
\frac{V}{L}\left(\frac{L}{2},\Delta\right) &= \frac{Y_1}{L}(\Delta), \text{ where}\\
\frac{w_q}{L}\left(\frac{L}{4},\Delta\right) &= 0.2651\frac{\Delta}{L},\\
\frac{w_q}{L}\left(\frac{L}{2},\Delta\right) &= 0.1996\frac{\Delta}{L}.
\end{aligned}$$

Here we take into account the contribution of the quasi-static motion w_q, (2), produced by the actuator of the cable [14, 19] to the in-plane displacement w. Furthermore, because we consider the maximum displacement, low damping, and no phase lag in response of the cable, in the equation for w_q, we use Δ/L instead of $\delta/L = (\Delta/L)\cos(\Omega t)$.

The in-plane quarter- and mid-point displacements along the stable branches l_1–l_4 are shown in Figs. 8a and b, and their out-of-plane quarter- and mid-point displacements in Fig. 8c and d. The white circles are measured experimental data points. For each data point the experiment was started at the rest position of the cable for the associated value of the excitation amplitude Δ/L. After transients died down, the in-plane and out-of-plane amplitudes at the quarter- and mid-points of the cable were measured; the maximum excitation amplitude that was considered was $\Delta/L = 2.33 \times 10^{-4}$. In all panels of Fig. 8 the measured amplitudes agree very well with the predicted values. In particular, the measurements shows that, up to the fold point F_1 at $\Delta/L \approx 2.0372 \times 10^{-4}$, the cable indeed displays practically zero in-plane amplitude at the mid point $L/2$, as well as no out-of-plane dynamics.

What is more, beyond the point F_1 the cable response changes its nature and out-of-plane modal amplitudes start contributing. Indeed, we measured nonzero out-of-plane amplitudes $V(L/4)$ and $V(L/2)$, as well as a considerably higher amplitude at $W(L/4)$. This experimental observation agrees well with the theoretical prediction. However, the prediction of the actual

measured amplitudes is less accurate for $\Delta/L > 2.0372 \times 10^{-4}$, that is, for solutions along the stable branch l_3. While $V(L/4)$ is predicted quite accurately, there is some mismatch in the measurements of $W(L/4)$ and $V(L/2)$; notice further that there is also a measured amplitude contribution of $W(L/2)$. We remark that, when out-of-plane dynamics of the response is present as well, determining the displacement at the in-plane and out-of-plane amplitudes at quarter- and mid-points reliably over a long period of time is quite a bit harder. We suspect that this difficulty may arise because of a weak interaction between the out-of-plane Y_1-amplitude and quasi-static in-plane motion. Notice further that the experiment needs to be run longer to allow transients to die down, which also introduces an additional level of uncertainly concerning the exact measured amplitudes.

In spite of these technical difficulties, overall Fig. 8 clearly shows that the displacements of the cable, even for Δ/L above F_1, are predicted well by the stable parts of solution branches found by numerical continuation for the averaged system (15) representing the vibration response of the vertically excited cable. More specifically, with the continuation technique it is possible to predict accurately when the response of the cable changes from uncoupled in-plane modal amplitude dynamics to dynamics with a contribution of the out-of plane modal amplitudes. Moreover, it is possible to predict from the four-mode model exactly which modal amplitudes are involved in these coupled responses and with which amplitudes.

5. Conclusions

In this paper we have presented a study of the nonlinear vibration of an inclined cable that is excited at its lower attachment point. This type of cable vibration is of interest because inclined cables are used to support the bridge deck in cable-stay bridges. Previous work had identified the lower stability boundaries for out-of-plane, sway motion in terms of the excitation amplitude and frequency, and validated them experimentally. In this paper we extended this work by (i) determining the stability diagram in the plane of excitation amplitude versus detuning, (ii) showing how additional stable branches are connected to known solutions via unstable branches, and (ii) deriving quantitative amplitude information for the modal displacements of the cable. These theoretical results are in good agreement with experimental measurements that go further than those in [13, 14] in that they also show the computed modal displacements of the cable.

6. Acknowledgments

The authors would like to acknowledge the support from the Engineering and Physical Sciences Research Council (EPSRC) of the research of Dr. M. R. Marsico and V. Tzanov under grant EP/F030711/1. We would like to thank Dr. M.S. Dietz for assisting with the experimental set-up, and the technicians at the Earthquake Engineering Laboratory for their assistance. We are also grateful to Dr J. H. G. Macdonald who gave us feedback on the experimental results and the manuscript.

References

[1] N. Srinil, G. Rega, S. Chucheepsakul, Three-dimensional non-linear coupling and dynamic tension in the large-amplitude free vibrations of arbitrarily sagged cables. *Journal of Sound & Vibration*, 269(3-5) (2004) 823–852.

[2] J. L. Lilien, A. P. Pinto Da Costa, Vibration amplitudes caused by parametric excitation of cable stayed structures. *Journal Sound & Vibration* 174 (1994) 69–90.

[3] T. Bakri, R. Nabergoj, A. Tonel, F. Verhulst, Parametric excitation in non-linear dynamics . *International Journal Non-linear Mechanics*, 39 (2004) 311–329.

[4] V. Gattulli, L. Martinelli, F. Perotti, F. Vestroni, Non-linear oscillations of cables under harmonic loading using analytical and finite element models. *Comput. Meth. Appl. Mech. Eng.*, 193 (2004) 69–85.

[5] V. Gattulli, M. Lepidi, J. Macdonald and C. Taylor, One-to-two global local interaction in a cable stayed beam observed through analytical, finite element and experimental models. *International Journal of Non-Linear Mechanics*, 40(5) (2005) 571–588 .

[6] Y. Fujino, P. Warnitchai and B.M. Pacheco, An experimental and analytical study of autoparametric resonance in a 3DOF model of cable-stayed-beam. *Nonlinear Dynam.*, 4 (1993) 111–138.

[7] G. Rega, W. Lacarbonara, A.H. Nayfeh, C.M. Chin, Multiple resonances in suspended cables: direct versus reduced-order models. *International Journal of Non-linear Mechanics*, 34(5) (1999) 901–924.

[8] G. Rega, Nonlinear vibrations of suspended cables- part i: Modeling and analysis. *Applied Mechanics Review*, 57 (2004) 443–478.

[9] G. Rega, Nonlinear vibrations of suspended cables- part ii: Deterministic phenomena. *Applied Mechanics Review* 57 (2004) 479–514.

[10] A. Berlioz, C. H. Lamarque, A non-linear model for the dynamics of an inclined cable. *Journal of Sound & Vibration*, 279(3-5) (2005) 619–639.

[11] N. Srinil, G. Rega, S. Chucheepsakul, Two-to-one resonant multi-modal dynamics of horizontal/inclined cables. part i: Theoretical formulation and model validation. *Nonlinear Dynamics*, 48(3) (2007) 231–252.

[12] N. Srinil, G. Rega, Two-to-one resonant multi-modal dynamics of horizontal/inclined cables. part ii: Internal resonance activation, reduced-order models and nonlinear normal modes. *Nonlinear Dynamics*, 48(3) (2007) 253–274.

[13] A. Gonzalez-Buelga, S.A. Neild, D.J. Wagg, J.H.G. Macdonald, Modal stability of inclined cables subjected to vertical support excitation. *Journal of Sound & Vibration*, 318 (2008) 565–579.

[14] J.H.G. Macdonald, M.S. Dietz, S.A. Neild, A. Gonzalez-Buelga, A.J. Crewe, D.J. Wagg, Generalised modal stability of inclined cables subjected to support excitations. *Journal of Sound & Vibration*, 329 (2010) 4515–4533.

[15] P. Warnitchai, Y. Fujino, B.M. Pacheco, A. Agret, An experimental study on active tendon control of cable-stayed bridges. *Earthquake Eng. Struct. Dynam.*, 22 (1993) 93–111.

[16] H. Irvine, *Cable structures*, MIT Press, Cambridge, MA. 1981.

[17] A.H. Nayfeh, P.F. Pai, *Linear and Nonlinear Structural Mechanics*, Wiley, 2004.

[18] P. Warnitchai, Y. Fujino, T. Susumpow, A nonlinear dynamic model for cables and its application to a cable structure system. *Journal of Sound & Vibration*, 187(4) (1995) 695–712.

[19] D. Wagg, S. Neild, *Nonlinear Vibration with Control*, Springer, 2010.

[20] E. Doedel, in *Numerical Continuation Methods for Dynamical Systems*, edited by B.Krauskopf, H. Osinga, and J. Galan-Vioque, Springer-Verlag, Dordrecht, 2007.

[21] E.J. Doedel, with major contributions from A.R. Champneys, T.F. Fairgrieve, Y.A. Kuznetsov, B. Sandstede, X.J. Wang, *AUTO2000 and AUTO-07P: Continuation and bifurcation software for ordinary differential equations*, Department of Computer Science, Concordia University, Montreal, Canada, 2000; available from `http://sourceforge.net/projects/auto2000`.

[22] C.L.S. Massow, Bifurcation and Numerical Integration Analysis of Parametric Excitation of Inclined Cables, PhD Thesis, Faculty of Engineering, University of Bristol, 2010.

[23] G. Rega, R. Alaggio, F. Benedettini, Experimental Investigation of the Nonlinear Response of a Hanging Cable. Part I: Local Analysis. *Nonlinear Dynamics*, 17 (1997) 89–117.

[24] G. Rega, N. Srinil, R. Alaggio, Experimetal and Numerical Studies of Inclined Cables: free and parametrically-forced vibrations. *Journal of Theoretical and Applied Mechanics*, 3(46) (2008) 621–640.

[25] G. Rega, R. Alaggio, Experimental unfolding of the nonlinear dynamics of a cable-mass suspended system around a divergence-Hopf bifurcation. *Journal of Sound & Vibration*, 322 (2009) 581–611.

[26] R. Lorenzo, J. Macdonald, Experimental validation of a simplified cable-stayed bridge model exhibiting autoparametric resonance, *In Proc. 5th Int. Symp. Cable Dynamics*, 2003, pp. 157–164.

[27] M.R. Marsico, J. Sieber, S. Neild, D.J. Wagg, Dynamic testing for uncertainty in structural dynamics, *Proceedings of 2nd International Conference on Uncertainty in Structural Dynamics*, The University of Sheffield, 2009.

[28] H.M. Irvine, T.K. Caughey, The linear theory of free vibrations of a suspended cable, *Proceedings of the Royal Society A*, 1974, pp. 299–315.

[29] N. Srinil, G. Rega, Nonlinear longitudinal/transversal modal interactions in highly extensible suspended cables. *Journal of Sound & Vibration*, 310(1-2) (2008) 230–242.

[30] F. Verhulst, *Nonlinear Differential Equations and Dynamical Systems*, Springer, 1996.

[31] M.R. Marsico, S. Neild, A. Gonzalez-Buelga, D. Wagg, Interaction between in-plane and out- of-plane cable mode for a cable-deck system, *Proceedings of ASME 2009 Design Engineering technical Conference and Computers and Information in Engineering Conference*, DETC2009.

[32] M.R. Marsico, D. Wagg, S. Neild, Stability for bridge cable and cable-deck interaction, *Proceedings of 3rd International Conference on Advances in Experimental Structural Engineering*, San Francisco, California, 2009.

[33] J. Guckenheimer, P. Holmes. *Nonlinear Oscillations, Dynamical Systems and Bifurcations of Vector Fields,* Springer-Verlag, New York/Berlin, second edition, 1986.

[34] Y.A. Kuznetsov *Elements of Applied Bifurcation Theory*, Springer-Verlag, New York/Berlin, second edition, 1998.

Figure Captions

- Figure 1: Schematic representation of an inclined cable with vertical input motion at the lower attachement point.

- Figure 2: Apparatus for inclined cable experiment: a) side view, b) looking along cable from bottom, c) hydraulic actuator and load cell. The cable is 5.4 m long, has diameter 0.00078 m and is inclined at 22.6°. The lead masses are applied to increase the cable mass for more realistic scaling. Deck excitation is simulated with the hydraulic actuator positioned at the lower attachment point.

- Figure 3: Partial stability diagram of Eqs. (15) in the $(\mu, \Delta/L)$-plane showing a curve F_{Z_2} of fold bifurcations of Z_2 and curves B_{Z_1} and B_{Y_1} of branch points of Z_1 and Y_1, respectively. Also shown are measured data points; here $\square$ indicates the largest Δ/L-value where only Z_2 was detected, $\triangle$ where Y_1 was detected for the first time, $\diamond$ where Z_1 was detected for the first time, and $\triangledown$ that Y_2 was detected.

- Figure 4: Stability diagram of Eqs. (15) in the $(\mu, \Delta/L)$-plane showing all bifurcation loci of Z_2-mode response: the curve F_{Z_2} of fold bifurcations and curves B_{Z_1}, B_{Y_1} and B_{Y_2} of branch point bifurcations; along solid parts of curves the bifurcation concerns a stable solutions and along dashed parts it concerns an unstable solution. The measured data points are repeated from Figure 3; panel b) is an enlargement for small Δ/L.

- Figure 5: Partial stability diagram of Eqs. (15) in the $(\mu, \Delta/L)$-plane showing the following bifurcation curves of (Z_2, Y_1, Y_2)-solutions:
  F^1 and F^2 - fold bifurcation curves, H^1 - Hopf point bifurcation curve. At F^1, F^2 and H^1, unstable (Z_2, Y_1, Y_2)-solutions meet stable (Z_2, Y_1, Y_2)-solutions. B^1 and B^2 - branch point bifurcation curves. At B^1, stable (Z_2, Y_1, Y_2)-solutions meet stable (Z_2, Y_1)-solutions, while at B^2, stable (Z_2, Y_2)-solutions meet stable (Z_2, Y_1, Y_2)-solutions.
  Also, shown are the points N, M, Q, R which represent the borders between the different bifurcation curves.

- Figure 6: One-parameter bifurcation diagram of Eqs. (15) for $\mu = 0.02$, showing solution branches represented by their norm $||N|| =$

$\sqrt{Z_1^2 + Z_2^2 + Y_1^2 + Y_2^2}/L$ for $\Delta/L \in [0, 6 \times 10^{-4}]$. The stable solution branches l_1–l_4 (black curves) are connected via unstable solution branches (grey curves), which meet at bifurcation points; specifically, The B_1, B_2, and B_3 are branch points (denoted by ■), F_1 and F_2 are fold points (denoted by ●), and H is a Hopf bifurcation point (denoted by $*$).

- Figure 7: Mode contributions to the stable branches l_1–l_4 from Figure 6, showing the contribution of a) Z_2, b) Z_1, c) Y_2, and d) Y_1.

- Figure 8: Comparison of theoretical maximum displacement with experimental measurments for $\mu = 0.02$. Shown are measured data points of displacement (denoted by ○), together with theoretical values along the stable branches l_1–l_4 of a) $w(\frac{L}{4})/L$, b) $w(\frac{L}{2})/L$, c) $v(\frac{L}{4})/L$, and d) $v(\frac{L}{2})/L$.

Table 1: Cable parameters; note that B, ξ and κ are nondimensional.

N_1 [Hz^2/m]	W_{12} [1/(s.m)^2]	ω_1 [rad/s]	B	ξ	κ
1.04×10^{-4}	5.19×10^{-4}	20.4852	0.2939	0.002	0.0234

Table 2: Cable natural frequencies.

	ω_{y1} [rad/s]	ω_{y2} [rad/s]	ω_{z1} [rad/s]	ω_{z2} [rad/s]
Experimental	$3.25 \cdot 2\pi$	$6.51 \cdot 2\pi$	$3.34 \cdot 2\pi$	$6.51 \cdot 2\pi$
Theoretical	$3.25 \cdot 2\pi$	$6.50 \cdot 2\pi$	$3.33 \cdot 2\pi$	$6.50 \cdot 2\pi$

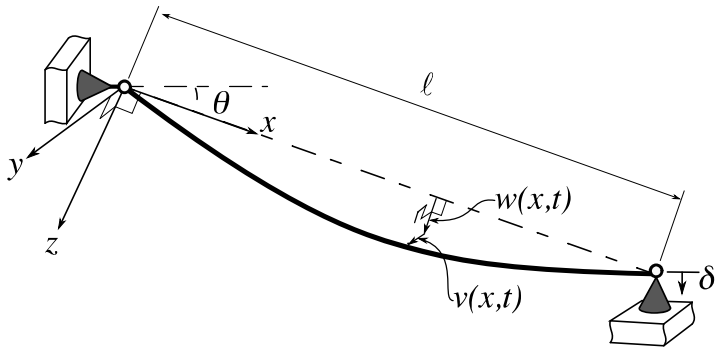

Figure 1: Schematic representation of an inclined cable with vertical input motion at the lower attachement point.

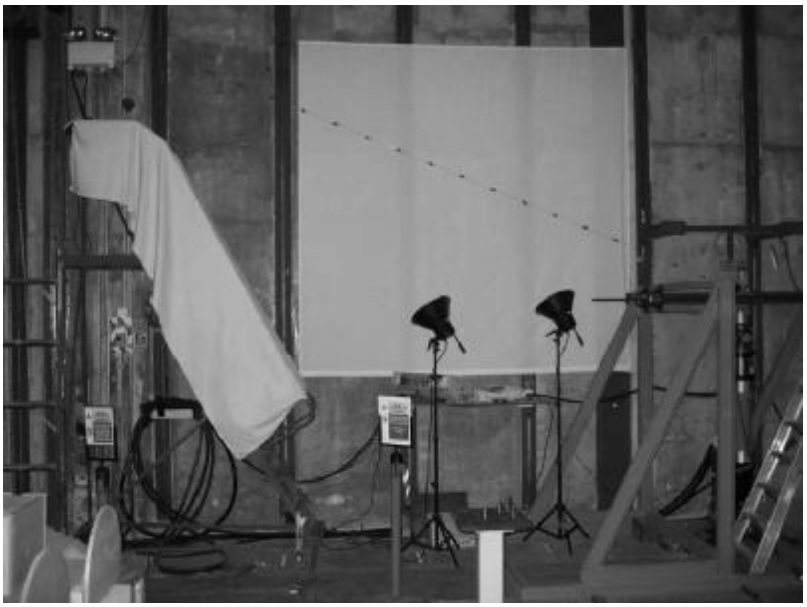

(a)

(b)

(c)

Figure 2: Apparatus for inclined cable experiment: a) side view, b) looking along cable from bottom, c) hydraulic actuator and load cell. The cable is 5.4 m long, has diameter 0.00078 m and is inclined at 22.6°. The lead masses are applied to increase the cable mass for more realistic scaling. Deck excitation is simulated with the hydraulic actuator positioned at the lower attachment point.

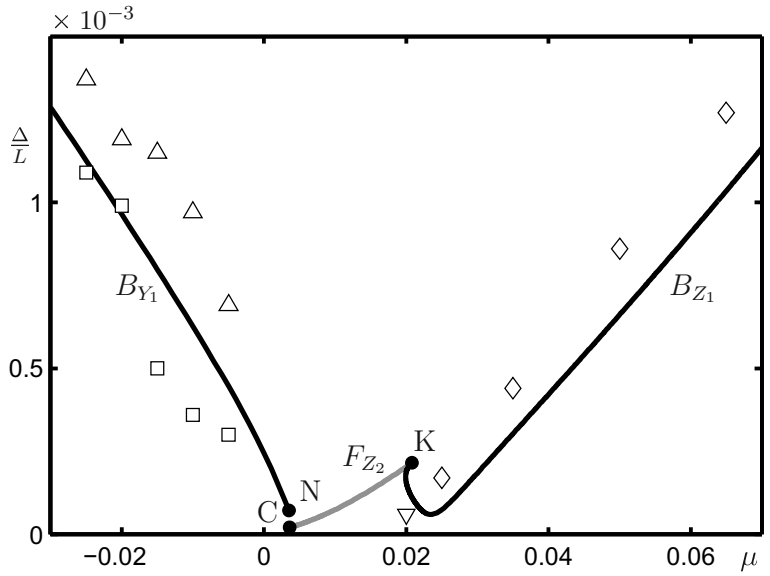

Figure 3: Partial stability diagram of Eqs. (15) in the $(\mu, \Delta/L)$-plane showing a curve F_{Z_2} of fold bifurcations of Z_2 and curves B_{Z_1} and B_{Y_1} of branch points of Z_1 and Y_1, respectively. Also shown are experimental data points; here $\square$ indicates the largest Δ/L-value where only Z_2 was detected, $\triangle$ where Y_1 was detected for the first time, $\diamond$ where Z_1 was detected for the first time, and $\triangledown$ that Y_2 was detected.

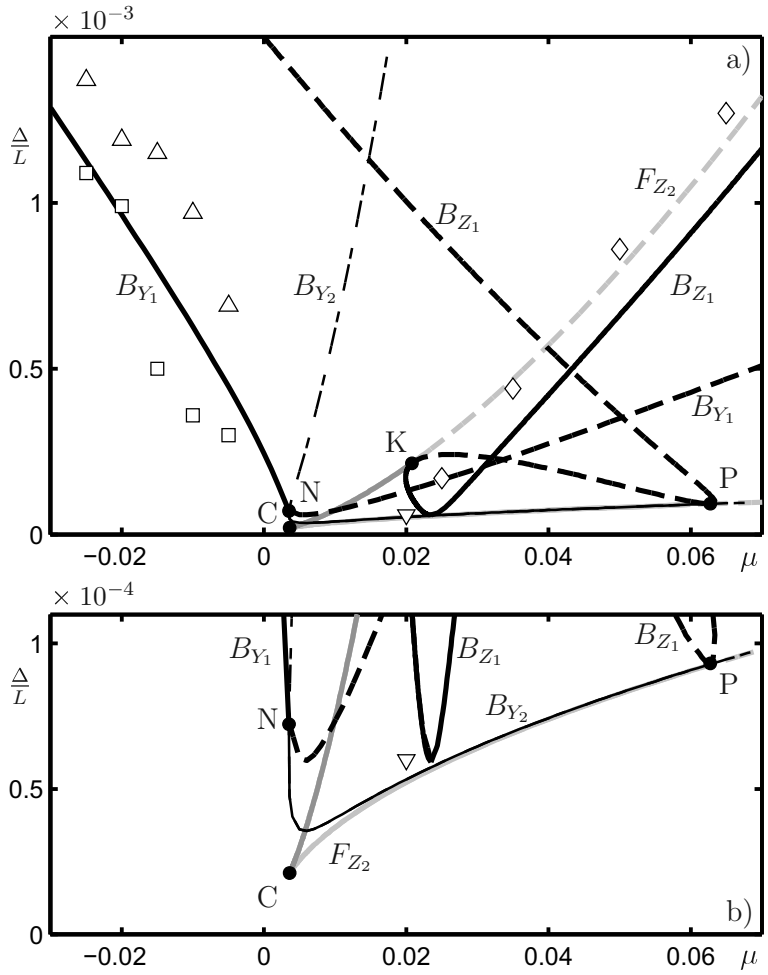

Figure 4: Stability diagram of Eqs. (15) in the $(\mu, \Delta/L)$-plane showing all bifurcation loci of Z_2-mode response: the curve F_{Z_2} of fold bifurcations and curves B_{Z_1}, B_{Y_1} and B_{Y_2} of branch point bifurcations; along solid parts of curves the bifurcation concerns a stable solutions and along dashed parts it concerns an unstable solution. The experimental data points are repeated from Figure 3; panel b) is an enlargement for small Δ/L.

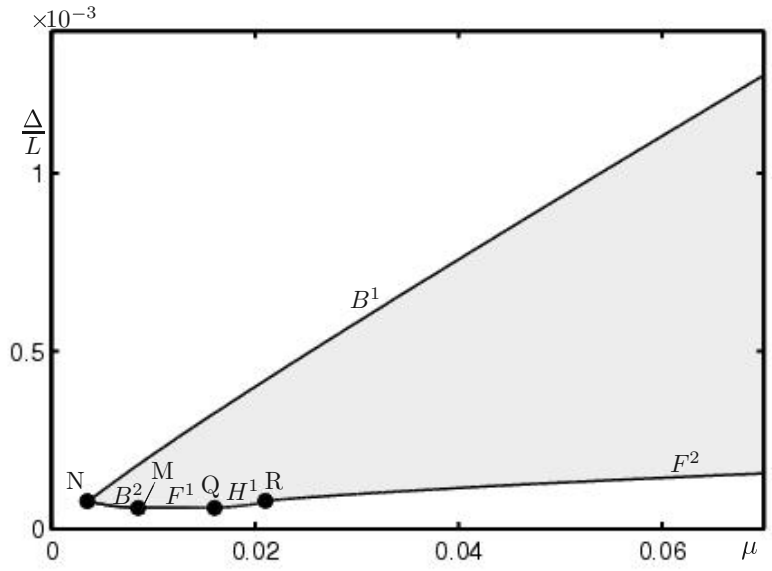

Figure 5: Partial stability diagram of Eqs. (15) in the $(\mu, \Delta/L)$-plane showing the following bifurcation curves of (Z_2, Y_1, Y_2)-solutions: F^1 and F^2 - fold bifurcation curves, H^1 - Hopf point bifurcation curve, at F^1, F^2 and H^1, unstable (Z_2, Y_1, Y_2)-solutions meet stable (Z_2, Y_1, Y_2)-solutions; B^1 and B^2 - branch point bifurcation curves, at B^1, stable (Z_2, Y_1, Y_2)-solutions meet stable (Z_2, Y_1)-solutions, while at B^2, stable (Z_2, Y_2)-solutions meet stable (Z_2, Y_1, Y_2)-solutions. Also, shown are the points N, M, Q, R which represent the borders between the different bifurcation curves.

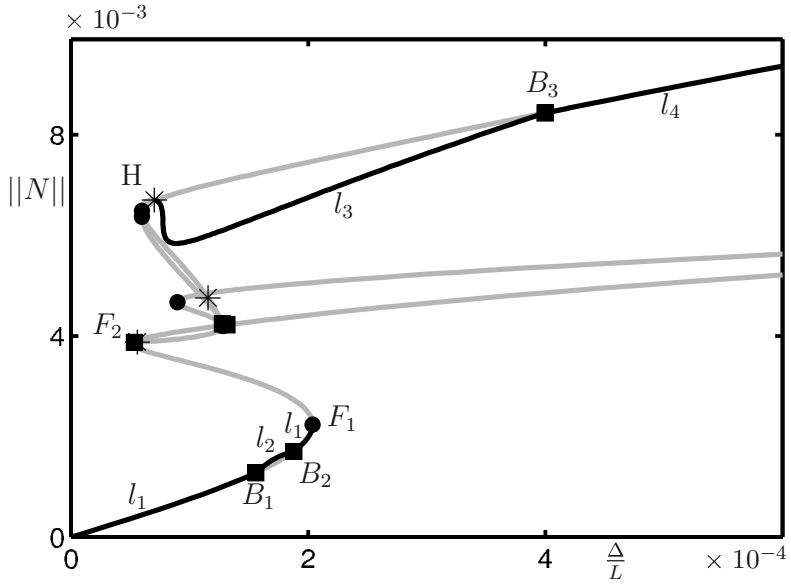

Figure 6: One-parameter bifurcation diagram of Eqs. (15) for $\mu = 0.02$, showing solution branches represented by their norm $||N|| = \sqrt{Z_1^2 + Z_2^2 + Y_1^2 + Y_2^2}/L$ for $\Delta/L \in [0, 6 \times 10^{-4}]$. The stable solution branches l_1–l_4 (black curves) are connected via unstable solution branches (grey curves), which meet at bifurcation points; specifically, The B_1, B_2, and B_3 are branch points (denoted by ■), F_1 and F_2 are fold points (denoted by ●), and H is a Hopf bifurcation point (denoted by $*$).

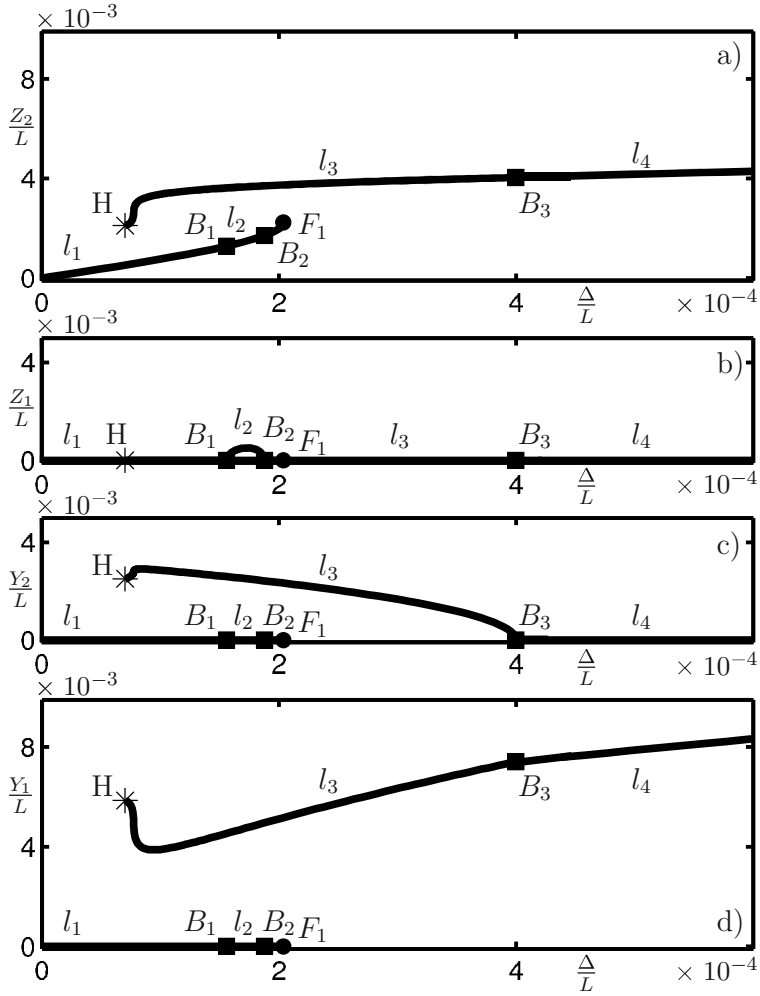

Figure 7: Mode contributions to the stable branches l_1–l_4 from Figure 6 ($\mu = 0.02$), showing the contribution of a) Z_2, b) Z_1, c) Y_2, and d) Y_1.

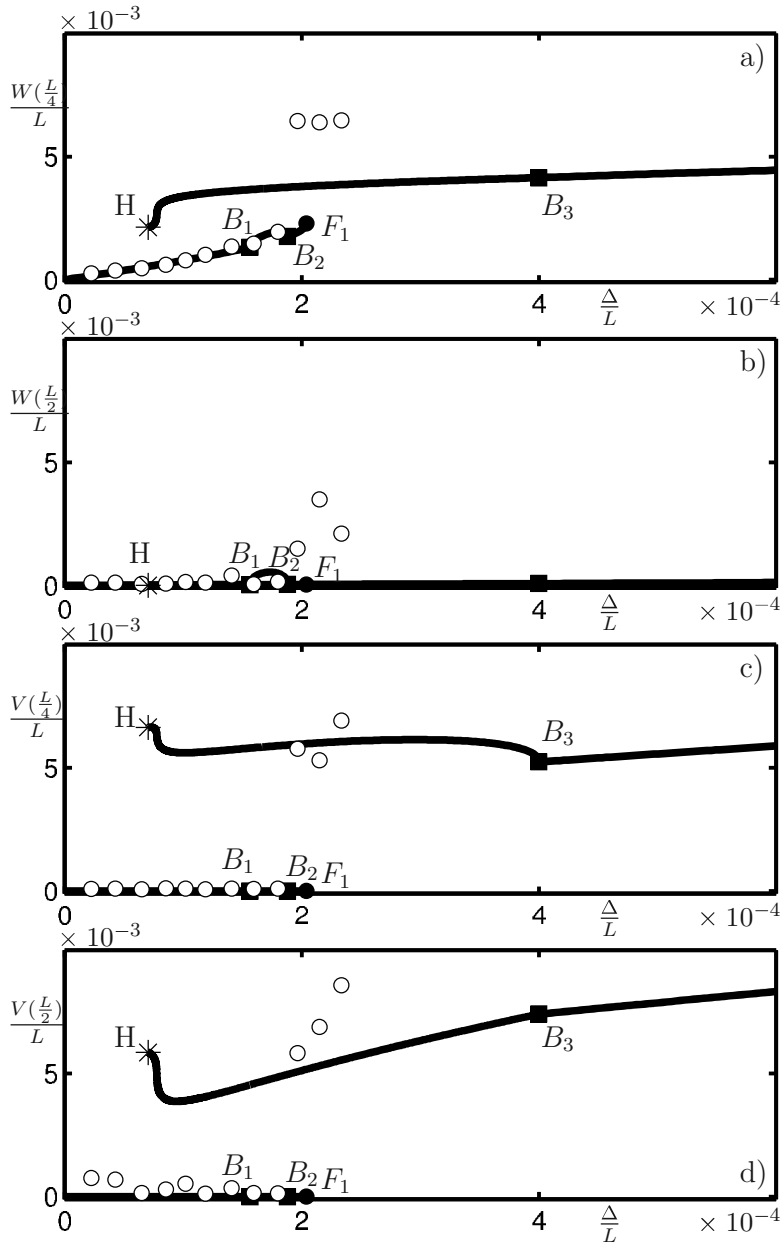

Figure 8: Comparison of theoretical maximum displacement with experimental measurments for $\mu = 0.02$. Shown are measured data points of displacement (denoted by $\bigcirc$), together with theoretical values along the stable branches l_1–l_4 of a) $W(\frac{L}{4})/L$, b) $W(\frac{L}{2})/L$, c) $V(\frac{L}{4})/L$, and d) $V(\frac{L}{2})/L$.